



# Photocatalytic degradation of gaseous toluene over hollow “spindle-like” $\alpha$ -Fe<sub>2</sub>O<sub>3</sub> loaded with Ag

Hong Li<sup>a,b</sup>, Qidong Zhao<sup>a</sup>, Xinyong Li<sup>a,d,\*</sup>, Yong Shi<sup>a</sup>, Zhengru Zhu<sup>c</sup>, Moses Tade<sup>d</sup>, Shaomin Liu<sup>d,\*\*</sup>

<sup>a</sup>State Key Laboratory of Fine Chemical, Key Laboratory of Industrial Ecology and Environmental Engineering (MOE), School of Environmental Science and Technology, Dalian University of Technology, Dalian 116024, China

<sup>b</sup>Department of Basic, Dalian Naval Academy, Dalian 116018, China

<sup>c</sup>Research Center of Hydrology and Engineering, Academy of City and Environment, Liaoning Normal University, Dalian 116029, China

<sup>d</sup>Department of Chemical Engineering, Curtin University, Perth, WA 6845, Australia

## ARTICLE INFO

### Article history:

Received 20 October 2011

Received in revised form 12 February 2012

Accepted 23 February 2012

Available online 3 March 2012

### Keywords:

A. Composites

B. Chemical synthesis

C. Electron microscopy

C. Infrared spectroscopy

D. Catalytic properties

## ABSTRACT

In this work, hollow “spindle-like”  $\alpha$ -Fe<sub>2</sub>O<sub>3</sub> nanoparticles were synthesized by a hydrothermal route. The Ag/ $\alpha$ -Fe<sub>2</sub>O<sub>3</sub> catalyst was prepared based on the spindle-shaped  $\alpha$ -Fe<sub>2</sub>O<sub>3</sub> with CTAB as the surfactant, which showed excellent photoelectric property and photocatalytic activity. The structural properties of these samples were systematically investigated by X-ray powder diffraction, scanning electronic microscopy, transmission electronic microscopy, energy-dispersive X-ray spectra, and UV–Vis diffuse reflectance spectroscopy techniques. The photo-induced charge separation in the samples was demonstrated by surface photovoltage measurement. The photocatalytic performances of the Ag/ $\alpha$ -Fe<sub>2</sub>O<sub>3</sub> and  $\alpha$ -Fe<sub>2</sub>O<sub>3</sub> samples were comparatively studied in the degradation of toluene under xenon lamp irradiation by in situ FTIR spectroscopy. Benzaldehyde and benzoic acid species could be observed on the  $\alpha$ -Fe<sub>2</sub>O<sub>3</sub> surface rather than Ag/ $\alpha$ -Fe<sub>2</sub>O<sub>3</sub> surface. The results indicate that the Ag/ $\alpha$ -Fe<sub>2</sub>O<sub>3</sub> sample exhibited higher photocatalytic efficiency.

© 2012 Elsevier Ltd. All rights reserved.

## 1. Introduction

Volatile aromatic compounds are particularly important constituents and comprise up to 44% of the volatile hydrocarbon mixture in the urban atmosphere [1]. Toluene is a major volatile aromatic pollutant. Various studies have tested the potential use of gas-phase photocatalytic oxidation of toluene for air detoxification [2–6]. The emphasis on photocatalytic oxidation of toluene has shifted toward the application of photocatalysis for air treatment [7]. Recently, increasing interest has grown in the photocatalytic oxidation of toluene by using visible-light active photocatalysts. Florea et al. [8] and Zhu et al. [9] reported the photooxidation of toluene over ferrite-type catalysts. Obee [10] reported the investigation of photooxidation of toluene and formaldehyde using another type of reactor, titania on glass-plate reactor and compared the results of two reactor designs.

From the viewpoint of solar energy utilization, the exploration of semiconductor photocatalysts that could utilize visible light

efficiently and possess proper band-gaps and advanced microscopic structure is still indispensable. As an important n-type semiconductor, hematite ( $\alpha$ -Fe<sub>2</sub>O<sub>3</sub>) is widely used for catalyst, chemical sensor, and magnetic applications due to its low cost, non-toxicity and high resistance to corrosion.  $\alpha$ -Fe<sub>2</sub>O<sub>3</sub> has also been selected as the support material for noble metal [11–14]. The notable advantages of supported noble metal catalysts are relatively high activity, mild process conditions, easy separation, and better handling properties. The choice of an efficient support could significantly improve the activity, selectivity, recycling, and reproducibility of Ag catalyst systems.

However, to date,  $\alpha$ -Fe<sub>2</sub>O<sub>3</sub> materials with various nanostructures have not been sufficiently explored. Many synthesis methods have been developed for the preparation of hematite ( $\alpha$ -Fe<sub>2</sub>O<sub>3</sub>) including sol–gel, hydrolysis of iron salt, solvothermal, and hydrothermal synthesis [15–18]. The catalytic properties depend on the morphology, particle size, and surface area, which are very sensitive to the preparation method used in their synthesis. The hydrothermal method is most favorable for its simplicity and good control of grain size in synthesizing magnetic oxides with controlled nanostructures.

In this study, hollow “spindle-like”  $\alpha$ -Fe<sub>2</sub>O<sub>3</sub> was fabricated by a facile hydrothermal method and then was employed as the support of Ag nanoparticles. After systematic characterization of the bulk and surface structures of hollow  $\alpha$ -Fe<sub>2</sub>O<sub>3</sub> and Ag/ $\alpha$ -Fe<sub>2</sub>O<sub>3</sub>

\* Corresponding author at: State Key Laboratory of Fine Chemical, Key Laboratory of Industrial Ecology and Environmental Engineering (MOE), School of Environmental Science and Technology, Dalian University of Technology, Dalian 116024, China. Tel.: +86 411 8470 7733; fax: +86 411 8470 7733.

\*\* Corresponding author. Tel.: +61 08 9266 9056; fax: +61 08 9266 2681.

E-mail addresses: [xyli@dlut.edu.cn](mailto:xyli@dlut.edu.cn) (X. Li), [shaomin.liu@curtin.edu.au](mailto:shaomin.liu@curtin.edu.au) (S. Liu).

catalytic materials, their performances in photocatalytic degradation of gaseous toluene and the detailed reaction mechanism were then comparatively studied by in situ FTIR spectroscopy. Positive effect of Ag species on the photocatalytic properties of Ag/ $\alpha$ -Fe<sub>2</sub>O<sub>3</sub> composite material was expected.

## 2. Experimental

### 2.1. Preparation of catalysts

All the materials were analytical grade reagents and used without further purification.

Hollow “spindle-like”  $\alpha$ -Fe<sub>2</sub>O<sub>3</sub> was obtained via a hydrothermal route. FeCl<sub>3</sub>·6H<sub>2</sub>O (18 mmol) was added into distilled water (60 mL) to form a clear solution. Then 4.32 g urea (CH<sub>4</sub>N<sub>2</sub>O) and 9 mL ethylene glycol, a protective agent were added into the solution. Subsequently under magnetic stirring for 30 min at room temperature, the resultant solution was put into a Teflon-lined stainless steel autoclave of 100 mL in capacity, which was sealed and maintained at 180 °C for 12 h. After cooling to room temperature naturally, the obtained precipitate was collected by filtration, and then washed with absolute ethanol and distilled water in sequence for several times. The final product was dried in a vacuum box at 80 °C for 12 h.

0.3335 g of as-prepared hollow spindle-shaped  $\alpha$ -Fe<sub>2</sub>O<sub>3</sub> was added into distilled water (20 mL) to form a solution under ultrasonic stirring for 10 min at room temperature. 0.45 g CTAB was added into the above solution, then after magnetic stirring for 30 min and ultrasonic stirring for 30 min, the solution was added into 25% NH<sub>3</sub>·H<sub>2</sub>O (3 mL) and 0.105 g AgNO<sub>3</sub> under magnetic stirring for 20 min at room temperature. Then the precipitation was collected by centrifugation, and washed with absolute ethanol and distilled water in sequence for several times. After evaporation, the catalyst was then dried at 100 °C for 12 h and calcined at 550 °C in air for 2 h followed by slow cooling under air atmosphere.

### 2.2. Characterizations

The phase structures of the  $\alpha$ -Fe<sub>2</sub>O<sub>3</sub> based samples prepared were determined by X-ray diffraction (XRD, RIGAKU, Dmax22000) with Cu K $\alpha$  radiation ( $\lambda = 0.15418$  nm) over the  $2\theta$  range of 20–80°. The morphology of the samples was investigated by scanning electronic microscopy (SEM) with a JSM-6700 LV electron microscope operating at 5.0 kV and transmission electron microscope (TEM, FEI Tecnai G<sup>2</sup>20). The compositions were examined by energy-dispersive X-ray spectroscopy (EDX) in the SEM. The amount of Ag dopant was determined by inductive coupling IPS-AEC (Optima 2000 DV, Perkin Elmer, USA). Light absorption property was examined using a UV-Vis diffuse reflectance spectrophotometer (JASCO, UV-550). The separation and transfer behaviors of the photogenerated charge carriers in the samples were investigated using a lock-in-based surface photovoltage (SPV) measurement system, which consists of a monochromator (model Omni- $\lambda$  3005) and a lock-in amplifier (model SR830-DSP) with an optical chopper (model SR540) running at a frequency of 20 Hz. All of the SPV measurements were performed at room temperature. The XPS data were recorded using an ESCALAB250 electron spectrometer using achromatic Al K $\alpha$  radiation (1486.6 eV) with Ar<sup>+</sup> sputtering to remove the surface layer of the sample.

### 2.3. Photocatalytic performance of the $\alpha$ -Fe<sub>2</sub>O<sub>3</sub> and Ag/ $\alpha$ -Fe<sub>2</sub>O<sub>3</sub> sample by GC and in situ FTIR

In situ FT-IR spectra were collected with a Fourier Transform Infrared Spectrophotometer (BRUKER VERTEX 70 Optics) and a self-made in situ IR quartz photoreaction cell [19]. The photocatalyst was

illuminated by an XQ-500W xenon lamp. The distance between the lamp and sample was about 15 cm. The light intensity at the sample holder was about 40.5 mW cm<sup>-2</sup>. Two pellets were prepared in parallel.

The reaction cell was purged by dry air for 1 h. After 1 h, the flux of dry air was set at 20 mL/min. Spectra of the clean catalyst surface were collected after this process and utilized as the background. Subsequently, toluene species was fed at the flow rate of 2  $\mu$ L/h for ca. 30 min using a syringe pump to a mixing tee where it was vaporized and mixed with the dry air. The reactant mixture then flowed through the reaction cell and allowed to equilibrate at room temperature (293 K). We determined whether the reactant concentration was stabilized by collecting its infrared spectrum every 5 min until a stable peak line on the infrared spectrum was obtained. Once the reactant concentration was stabilized, the inlet and outlet ports were shut off and the lamps were turned on. The infrared spectra were continuously collected during the reaction. The infrared spectra were collected with a resolution of 1 cm<sup>-1</sup> and 20 scans in the region of 4000–1000 cm<sup>-1</sup>.

The reactant concentration was measured by gas chromatography (Aligent 7890A, USA). During the reaction process, samples of approximately 1  $\mu$ L at the outlet every 0.5 h, were collected and the change in concentration of toluene was analyzed by a gas chromatography equipped with FID (HP-5 capillary column (30 m  $\times$  320  $\mu$ m  $\times$  0.25 m)) and TCD (Porapak Q). When the peak intensity of toluene did not obviously change, the xenon lamp was turned off and the cell was purified with the nitrogen.

## 3. Results and discussion

### 3.1. XRD analysis

The X-ray diffraction patterns of  $\alpha$ -Fe<sub>2</sub>O<sub>3</sub> and Ag/ $\alpha$ -Fe<sub>2</sub>O<sub>3</sub> samples are shown in Fig. 1. Seven major characteristic peaks can be indexed as the rhombohedral structure (JCPDS 84-0311) [20], which indicates the  $\alpha$ -Fe<sub>2</sub>O<sub>3</sub> phase with high purity and crystallinity (Fig. 1). No peaks from other phases are found, suggesting that the as-synthesized sample is pure highly. The characteristic peaks at  $2\theta$  of 24.18°, 33.15°, 35.75°, 40.93°, 49.43°, 54.02°, 57.56°, 62.51°, 64.05°, 71.94° and 75.48° are corresponding to (0 1 2), (1 0 4), (1 1 0), (1 1 3), (0 2 4), (1 1 6), (0 1 8), (2 1 4), (3 0 0), (0 1 1 0) and (2 2 0) crystallographic nucleation planes of hematite phase, respectively. In addition, the peak of (1 0 4) planes at  $2\theta = 33.15^\circ$  indicated a fine preferential growth of the  $\alpha$ -Fe<sub>2</sub>O<sub>3</sub> sample in the (1 0 4) direction. Two peaks of (1 1 1) and (2 0 0) planes corresponding to Ag species (JCPD No. 00-004-0783) could

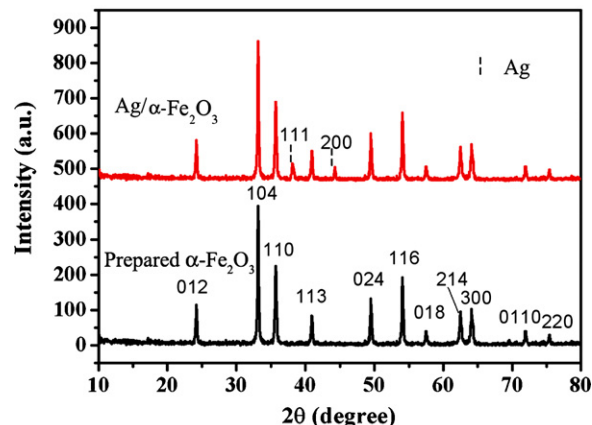


Fig. 1. The X-ray diffraction patterns of  $\alpha$ -Fe<sub>2</sub>O<sub>3</sub> and Ag/ $\alpha$ -Fe<sub>2</sub>O<sub>3</sub> samples.

be observed in the X-ray diffraction patterns (Fig. 1). From ICP analysis, 0.632 wt% Ag was loaded into the  $\alpha$ -Fe<sub>2</sub>O<sub>3</sub> sample.

As calculated from the XRD line broadening of the (1 0 4) peak using the Scherrer equation  $D = 0.89\lambda / \beta \cos \theta$ , the average sizes of the  $\alpha$ -Fe<sub>2</sub>O<sub>3</sub> and Ag/ $\alpha$ -Fe<sub>2</sub>O<sub>3</sub> samples are ca. 27 nm and 21 nm, respectively. The crystallite size of Ag/ $\alpha$ -Fe<sub>2</sub>O<sub>3</sub> sample seems to decrease with Ag loading. Previously, the crystallite size of mesoporous TiO<sub>2</sub> was also found to become smaller with Ag

doping [21]. Herein, the decreased crystallite size of  $\alpha$ -Fe<sub>2</sub>O<sub>3</sub> with Ag loading was probably due to the ultrasonic treatment, which destroyed some of the  $\alpha$ -Fe<sub>2</sub>O<sub>3</sub> particles into smaller ones.

### 3.2. SEM and TEM analysis

The SEM and TEM images in Fig. 2a–d show the morphology of the  $\alpha$ -Fe<sub>2</sub>O<sub>3</sub> and Ag/ $\alpha$ -Fe<sub>2</sub>O<sub>3</sub> samples, respectively. The two samples

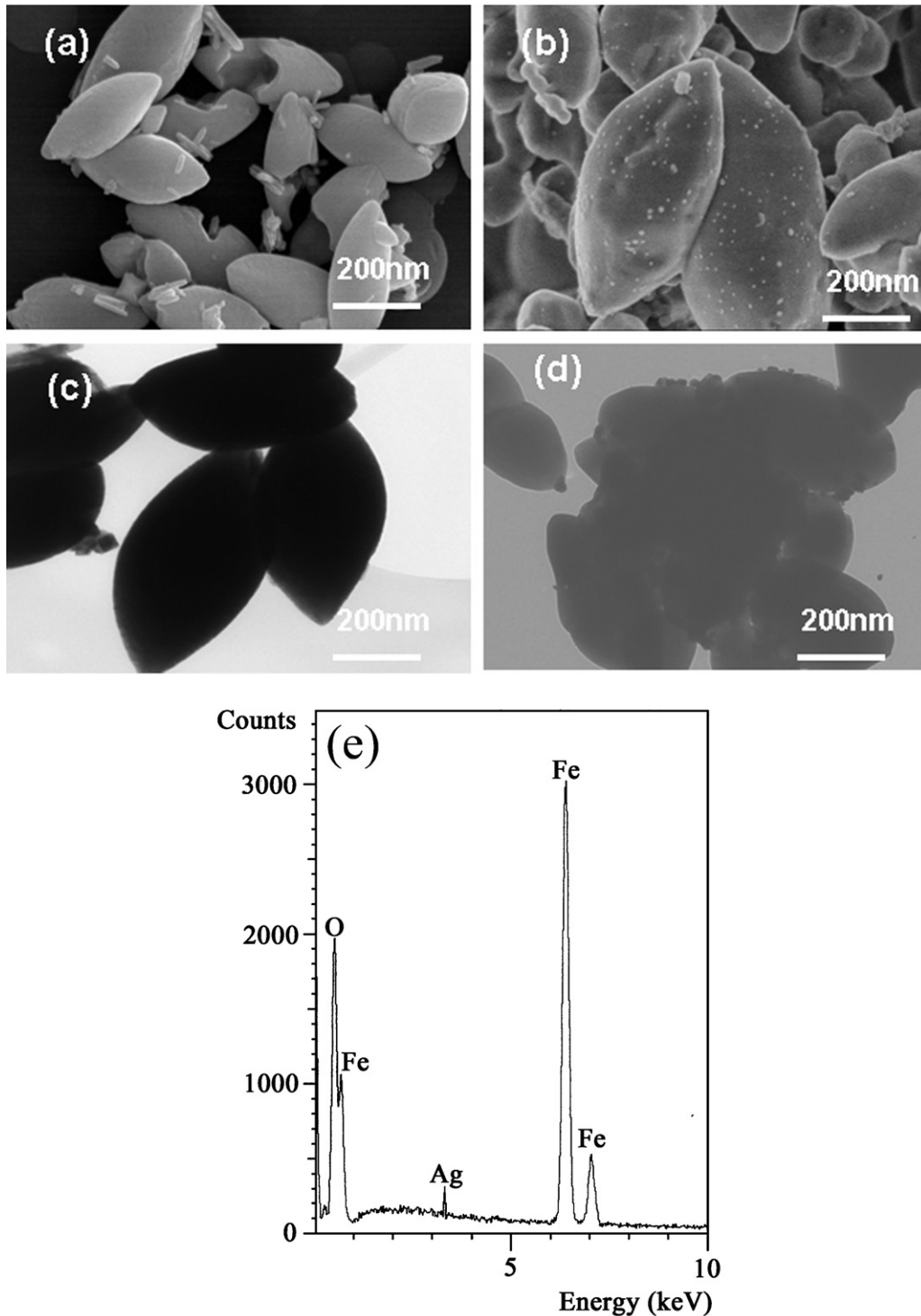


**Fig. 2.** The SEM images of the  $\alpha$ -Fe<sub>2</sub>O<sub>3</sub> (a) and Ag/ $\alpha$ -Fe<sub>2</sub>O<sub>3</sub> samples (b), the TEM images of the  $\alpha$ -Fe<sub>2</sub>O<sub>3</sub> (c) and Ag/ $\alpha$ -Fe<sub>2</sub>O<sub>3</sub> samples (d), and EDS spectrum of the Ag/ $\alpha$ -Fe<sub>2</sub>O<sub>3</sub> sample (e).

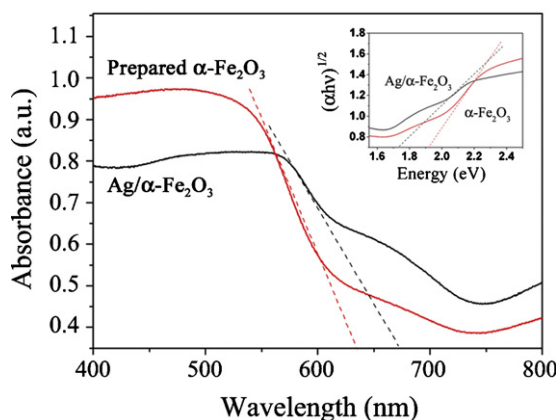


Fig. 3. The UV-Vis absorption spectra and  $(\alpha h\nu)^{1/2}$  vs.  $h\nu$  curve (inset) of the  $\alpha$ - $\text{Fe}_2\text{O}_3$  and  $\text{Ag}/\alpha$ - $\text{Fe}_2\text{O}_3$  samples.

are completely composed of hollow “spindle-like” particles. It could also be seen that spindle-shaped samples have the dimension size of micrometer. Statistical analysis of dimensional distributions (shown in Fig. 2c and d) based on TEM indicates that the length and the width are about 1.5  $\mu\text{m}$  and 0.5  $\mu\text{m}$ , respectively.

Fig. 2d shows the TEM micrograph of  $\text{Ag}/\alpha$ - $\text{Fe}_2\text{O}_3$  samples. As shown by the image, some dots exist on the surface of the sample distinctly. Hence, we can distinguish the Ag particles from the spindle-like support. The EDX patterns of the synthesized  $\text{Ag}/\alpha$ - $\text{Fe}_2\text{O}_3$  sample were taken to screen the composition of the metal. Metallic silver was successfully identified by referring to the corresponding EDX patterns of the samples (Fig. 2e).

### 3.3. DRS analysis

The UV-Vis absorption spectra of the  $\alpha$ - $\text{Fe}_2\text{O}_3$  and  $\text{Ag}/\alpha$ - $\text{Fe}_2\text{O}_3$  samples are given in Fig. 3. A more broad and strong absorption with the absorption edge at about 674 nm was found for  $\text{Ag}/\alpha$ - $\text{Fe}_2\text{O}_3$  sample, which absorbed more visible light than  $\alpha$ - $\text{Fe}_2\text{O}_3$ . The inset in Fig. 3 shows a plot of  $(\alpha h\nu)^{1/2}$  against the energy of absorbed light, from which the direct allowed band gaps can be estimated. Using this method, the estimated band gap of the  $\text{Ag}/\alpha$ - $\text{Fe}_2\text{O}_3$  sample is found to be 1.7 eV. Compared with the reported band gap values of  $\alpha$ - $\text{Fe}_2\text{O}_3$  (1.95 eV) and bulk  $\alpha$ - $\text{Fe}_2\text{O}_3$  (2.2 eV) [22], the absorption edge of the  $\alpha$ - $\text{Fe}_2\text{O}_3$  sample is red-shifted. Therefore, a better absorption capability of visible light is obtained with the  $\text{Ag}/\alpha$ - $\text{Fe}_2\text{O}_3$  sample.

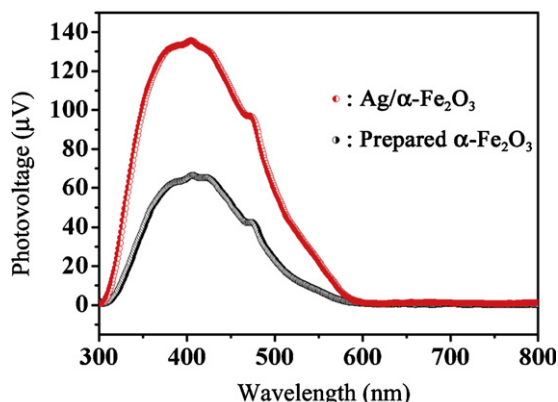


Fig. 4. The SPV spectra of the prepared  $\alpha$ - $\text{Fe}_2\text{O}_3$  and  $\text{Ag}/\alpha$ - $\text{Fe}_2\text{O}_3$  samples.

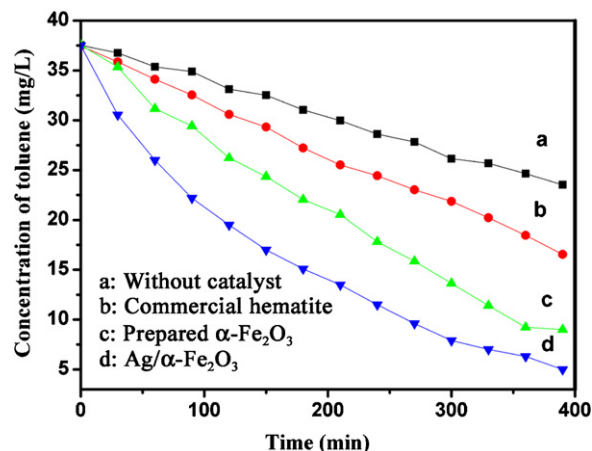


Fig. 5. The photocatalytic oxidation of toluene over the commercial  $\alpha$ - $\text{Fe}_2\text{O}_3$ , fabricated  $\alpha$ - $\text{Fe}_2\text{O}_3$ , and  $\text{Ag}/\alpha$ - $\text{Fe}_2\text{O}_3$  samples after the reaction proceeding for 6 h under xenon lamp irradiation conditions.

### 3.4. SPV analysis

The SPV technique can provide a rapid, nondestructive monitor of the surface properties of semiconductors [23]. Fig. 4 shows the SPV spectra of the  $\alpha$ - $\text{Fe}_2\text{O}_3$  and  $\text{Ag}/\alpha$ - $\text{Fe}_2\text{O}_3$  samples. It could be observed by systematic comparison of the change of the SPV spectra that the  $\text{Ag}/\alpha$ - $\text{Fe}_2\text{O}_3$  sample exhibits a more distinguished SPV response, and its performance is evidently higher than the  $\alpha$ - $\text{Fe}_2\text{O}_3$  sample. Hence, the higher photocatalytic activity might be expected for  $\text{Ag}/\alpha$ - $\text{Fe}_2\text{O}_3$  sample. Probably, the Ag species adsorbed onto the surface of  $\alpha$ - $\text{Fe}_2\text{O}_3$  play a key role in trapping the photo-generated electrons, which is due to that the Fermi level of Ag (ca.  $-4.3$  eV) [24] is much lower than the conduction band edge of the  $\alpha$ - $\text{Fe}_2\text{O}_3$  nanocrystals in electronic energy.

### 3.5. The photocatalytic properties of the $\alpha$ - $\text{Fe}_2\text{O}_3$ and $\text{Ag}/\alpha$ - $\text{Fe}_2\text{O}_3$ samples for degradation of gaseous toluene by GC analysis and in situ study

Fig. 5 shows the photocatalytic oxidation of toluene over the as-prepared  $\alpha$ - $\text{Fe}_2\text{O}_3$  and  $\text{Ag}/\alpha$ - $\text{Fe}_2\text{O}_3$  samples after the reaction proceeding for 6 h under xenon lamp irradiation conditions. The initial concentration of 100 ppm for toluene was used for reaction. The degradation percentage of toluene reaches up to 88%, whereas the degradation percentage of toluene over commercial  $\alpha$ - $\text{Fe}_2\text{O}_3$ , fresh  $\alpha$ - $\text{Fe}_2\text{O}_3$ , and without any catalyst reaches to 56%, 77% and 37%, respectively (see Fig. 5). It is obviously seen that the photocatalytic activity of the  $\text{Ag}/\alpha$ - $\text{Fe}_2\text{O}_3$  sample is more active than that of the  $\alpha$ - $\text{Fe}_2\text{O}_3$  sample.

We ascribe the enhanced photocatalytic activity of  $\text{Ag}/\alpha$ - $\text{Fe}_2\text{O}_3$  sample to a synergistic effect between loaded Ag species and the hollow supports. Firstly, the loaded silver content could not change the band gap of  $\alpha$ - $\text{Fe}_2\text{O}_3$ , but induce a more intensive absorption band in the visible-light range instead. Hence, we believe that the loaded Ag on the surface of the  $\alpha$ - $\text{Fe}_2\text{O}_3$  might be excited by proper incident photons, producing excitons via the plasmon effect [25]. There is certain possibility that the excitons dissociate. Some of the yielded charges could transfer across the interface between Ag nanoparticle and the  $\alpha$ - $\text{Fe}_2\text{O}_3$  support, contributing to the formation of active species at the surface. In addition, the excited electrons in the CB of  $\alpha$ - $\text{Fe}_2\text{O}_3$  would be trapped by Ag species adsorbed onto the surface of  $\alpha$ - $\text{Fe}_2\text{O}_3$ , and the Ag could enhance the separation of the photo-generated electrons from the holes, which would subsequently help form active radicals to degrade the

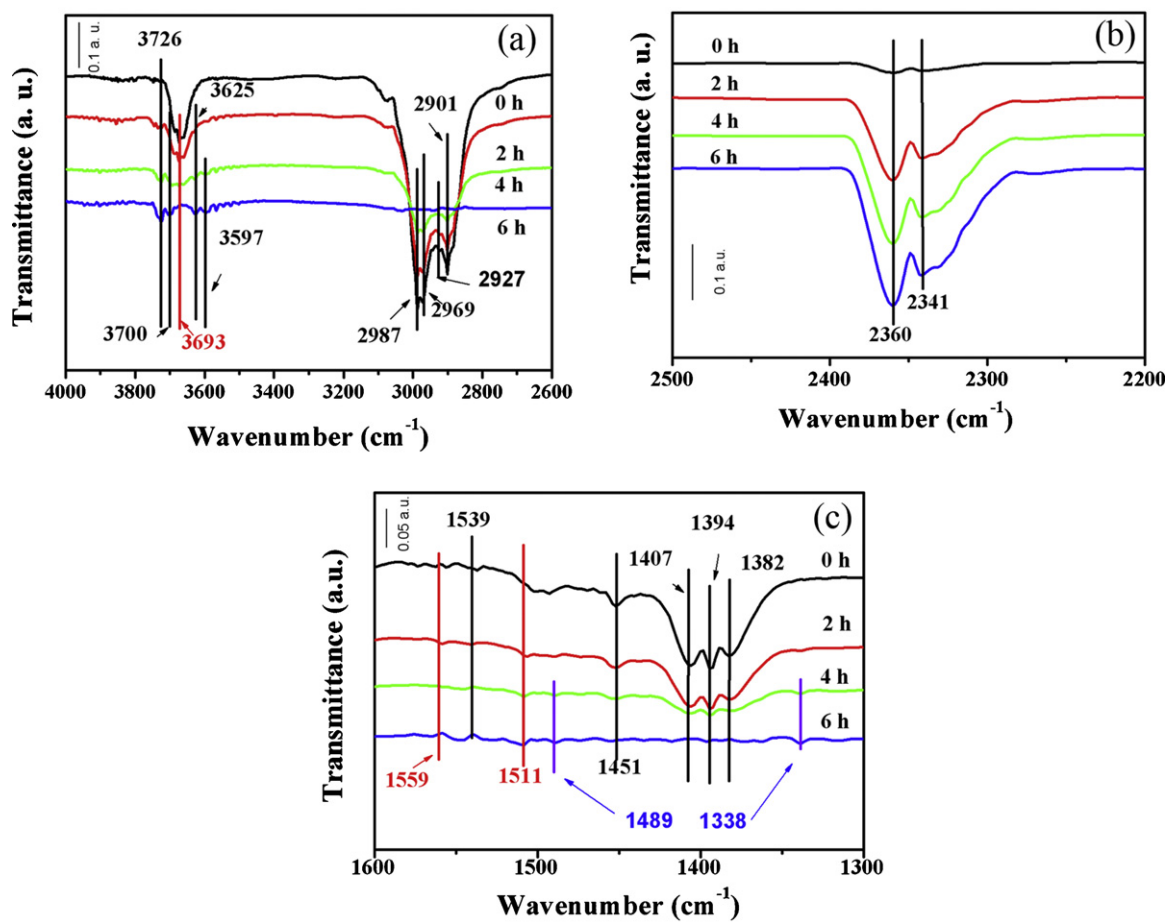


Fig. 6. The infrared absorbance spectra of toluene over the  $\alpha$ - $\text{Fe}_2\text{O}_3$  sample under xenon lamp irradiation for 6 h.

adsorbed pollutants. The above discussion explains the reason why  $\text{Ag}/\alpha\text{-Fe}_2\text{O}_3$  catalyst is much more active than the  $\alpha\text{-Fe}_2\text{O}_3$  sample.

### 3.6. In situ FTIR study of photodegradation mechanism of toluene

In situ infrared reaction study provides real-time monitoring of transient events which are occurring on the catalyst during the reaction. A set of infrared absorbance spectra obtains during the photocatalytic oxidation of toluene over  $\alpha\text{-Fe}_2\text{O}_3$  and  $\text{Ag}/\alpha\text{-Fe}_2\text{O}_3$  samples are shown in Figs. 6 and 7, respectively. The spectra were collected using the  $\alpha\text{-Fe}_2\text{O}_3$  and  $\text{Ag}/\alpha\text{-Fe}_2\text{O}_3$  samples as the background, respectively. Prior to xenon lamp illumination ( $t=0$ ), the spectrum displays the characteristic toluene bands at  $2987\text{ cm}^{-1}$ ,  $2969\text{ cm}^{-1}$ ,  $2927\text{ cm}^{-1}$ ,  $2901\text{ cm}^{-1}$ ,  $2901\text{ cm}^{-1}$ ,  $1539\text{ cm}^{-1}$ ,  $1451\text{ cm}^{-1}$ ,  $1407\text{ cm}^{-1}$ ,  $1394\text{ cm}^{-1}$  and  $1382\text{ cm}^{-1}$  [26], respectively. Upon irradiation, the intensity of these peaks began to decrease slowly. The signal corresponding to  $\text{CO}_2$  ( $2362\text{ cm}^{-1}$  and  $2340\text{ cm}^{-1}$ ) increased as the reaction progressed (Figs. 6c and 7c). The photocatalytic oxidation pathway of toluene over commercial  $\alpha\text{-Fe}_2\text{O}_3$  catalyst looks pretty similar (data not shown) (Fig. 6).

The FTIR spectra display a marked increase of the broad absorption in the  $3800\text{--}2800\text{ cm}^{-1}$  range, indicating the regeneration of interacting hydroxyl groups and adsorbed molecules on the sample surface, a small increase of the isolated hydroxyl bands, mainly the one at  $3690\text{ cm}^{-1}$  is observed. The results indicated that some adsorbed surface species molecules are released from the adsorption sites but probably remain on the

$\alpha\text{-Fe}_2\text{O}_3$  and  $\text{Ag}/\alpha\text{-Fe}_2\text{O}_3$  samples surface by water incorporation (Figs. 6b and 7b).

For Fig. 6, some bands related to the adsorbed water and hydroxyl groups [27] in the range of  $1300\text{--}1800\text{ cm}^{-1}$ . The band in the region of  $1260\text{--}1410\text{ cm}^{-1}$  could be assigned to be the corresponding aliphatic C–H bending vibration. After 2 h of illumination, the formation of several small bands in the  $1900\text{--}1100\text{ cm}^{-1}$  range ( $1559\text{ cm}^{-1}$ ,  $1511\text{ cm}^{-1}$ ,  $1489\text{ cm}^{-1}$  and  $1338\text{ cm}^{-1}$ ). Similar bands have been reported for benzaldehyde adsorption on nanostructured  $\text{TiO}_2$  and Degussa P25 [27–29]. As the irradiation time was increased, new bands appeared at  $1489\text{ cm}^{-1}$  and  $1338\text{ cm}^{-1}$ . These results indicate that weakly adsorbed benzaldehyde was formed as the reaction progressed [30]. Benzaldehyde molecules resulting from the photo-oxidation of toluene weakly interact with the catalyst surface so that they can be released to the gas phase. By contrast, hydroxyl groups on the surface of  $\alpha\text{-Fe}_2\text{O}_3$  are able to react with photo-produced benzaldehyde, which is then retained on the catalyst surface. Subsequently it can be converted into other products, like benzoic acid ( $1489\text{ cm}^{-1}$  and  $1338\text{ cm}^{-1}$ ) [31], which adsorbed on the  $\alpha\text{-Fe}_2\text{O}_3$  surface, leading to the progressive deactivation of the catalyst in the gas-solid system. These hydroxyl groups play a key role in the photocatalytic process and then this dehydroxylation should be responsible for the deactivation observed in the reaction carried out in the absence of water vapor.

Insights on the behaviors of the surface species of the  $\alpha\text{-Fe}_2\text{O}_3$  and  $\text{Ag}/\alpha\text{-Fe}_2\text{O}_3$  samples during the photo-oxidation process were obtained by analyzing the high frequency region of the spectrum of the catalyst, where the absorptions due to the stretches of

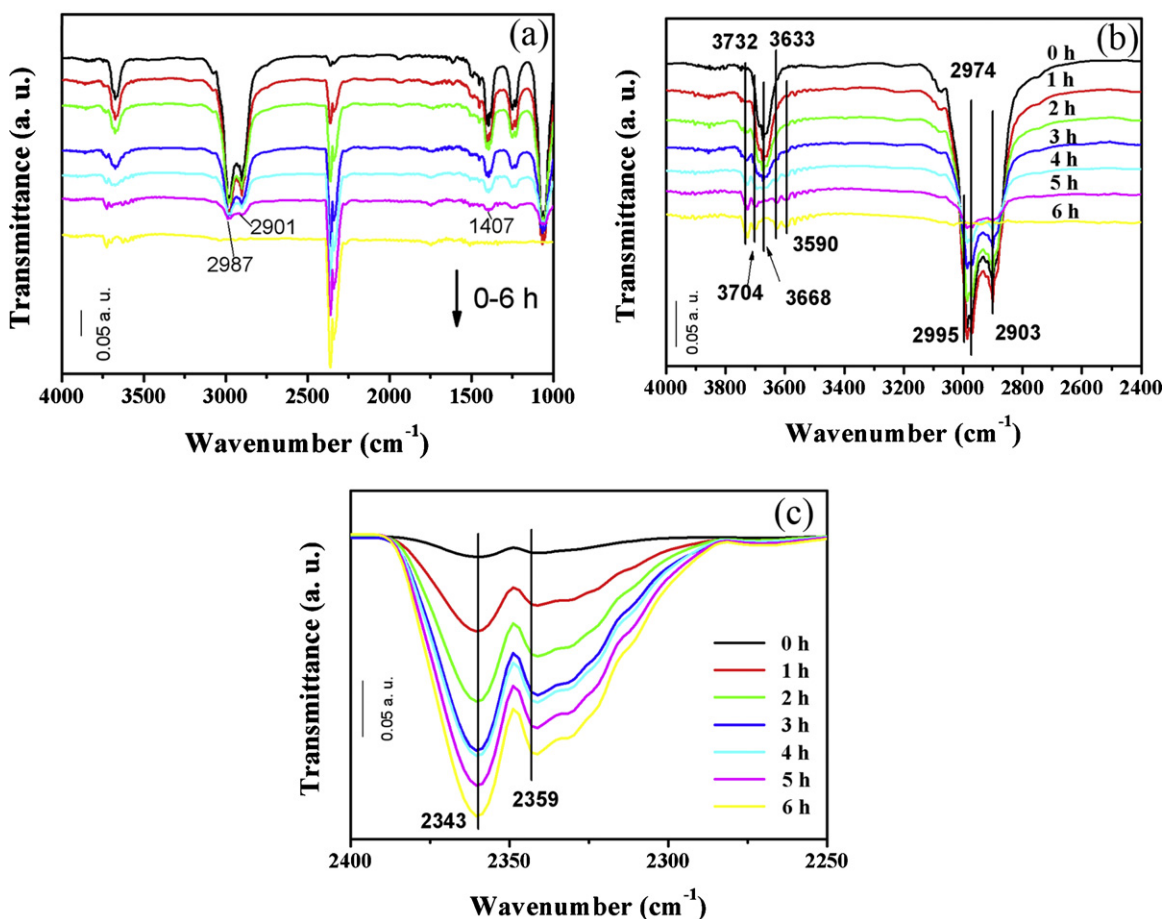


Fig. 7. The infrared absorbance spectra of toluene over the Ag/ $\alpha$ -Fe<sub>2</sub>O<sub>3</sub> sample under xenon lamp irradiation for 6 h.

hydroxyl groups and adsorbed water molecules are observed. The spectrum of the catalyst exhibits an asymmetric peak at 3672 cm<sup>-1</sup>, due to the stretching mode of free hydroxyl groups. The broad band at 3700–3500 cm<sup>-1</sup> (Fig. 6), resulting from the overlap of the bands is ascribed to the stretching modes of hydrogen bonded –OH groups and water molecules coordinated to surface Fe<sup>3+</sup> cations [30,31,6].

For Fig. 7, no bands assigned to be immediate species appeared during the reaction. This indicates that complete degradation of

toluene occurred on the Ag/ $\alpha$ -Fe<sub>2</sub>O<sub>3</sub> surface under the experimental conditions used. These results show that toluene was mineralized into carbon dioxide and water as the major species. However, only a partial oxidation was achieved on the  $\alpha$ -Fe<sub>2</sub>O<sub>3</sub> surface, due to benzaldehyde and benzoic acid species adsorbed on the  $\alpha$ -Fe<sub>2</sub>O<sub>3</sub> surface, leading to the progressive deactivation of the catalyst in the gas–solid system.

### 3.7. Study on the stability of the catalyst Ag/ $\alpha$ -Fe<sub>2</sub>O<sub>3</sub>

We carried out the experiments on the stability of the catalyst Ag/ $\alpha$ -Fe<sub>2</sub>O<sub>3</sub> for toluene photodegradation. Every repetition experiment lasted up to 6 h under the same in situ FT-IR test condition. The photodegradation ratio of the substrate was measured as a function of time for the Ag/ $\alpha$ -Fe<sub>2</sub>O<sub>3</sub> catalyst. The results are shown in Fig. 8. It is found that the photodegradation ratio of toluene reaches to 76% after the fifth repetition, which is slightly lower than that (88%) with the fresh Ag/ $\alpha$ -Fe<sub>2</sub>O<sub>3</sub> catalyst. The results show that the Ag/ $\alpha$ -Fe<sub>2</sub>O<sub>3</sub> catalyst has good stability and reusability.

In order to get a better understanding of the stability of the obtained composite Ag/Fe<sub>2</sub>O<sub>3</sub> catalyst, additional XPS analysis of the fresh and used Ag/Fe<sub>2</sub>O<sub>3</sub> samples was performed and the results are shown in Fig. 9. Fig. 9b shows the high-resolution XPS spectrum of the Ag in the fresh Ag/Fe<sub>2</sub>O<sub>3</sub>. The spectrum provides the binding energies of the Ag 3d<sub>3/2</sub> and Ag 3d<sub>5/2</sub> peaks as 374.6 and 368.7 eV, respectively, which reveals that the Ag species exists predominantly in the metallic form [32]. Meanwhile, the 6.0 eV gap between the two states is also characteristics of metallic Ag.

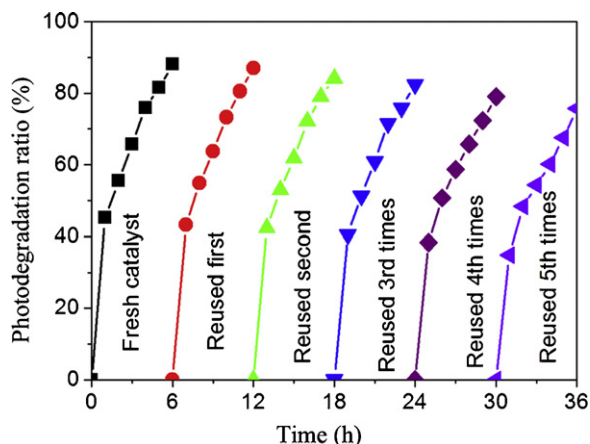
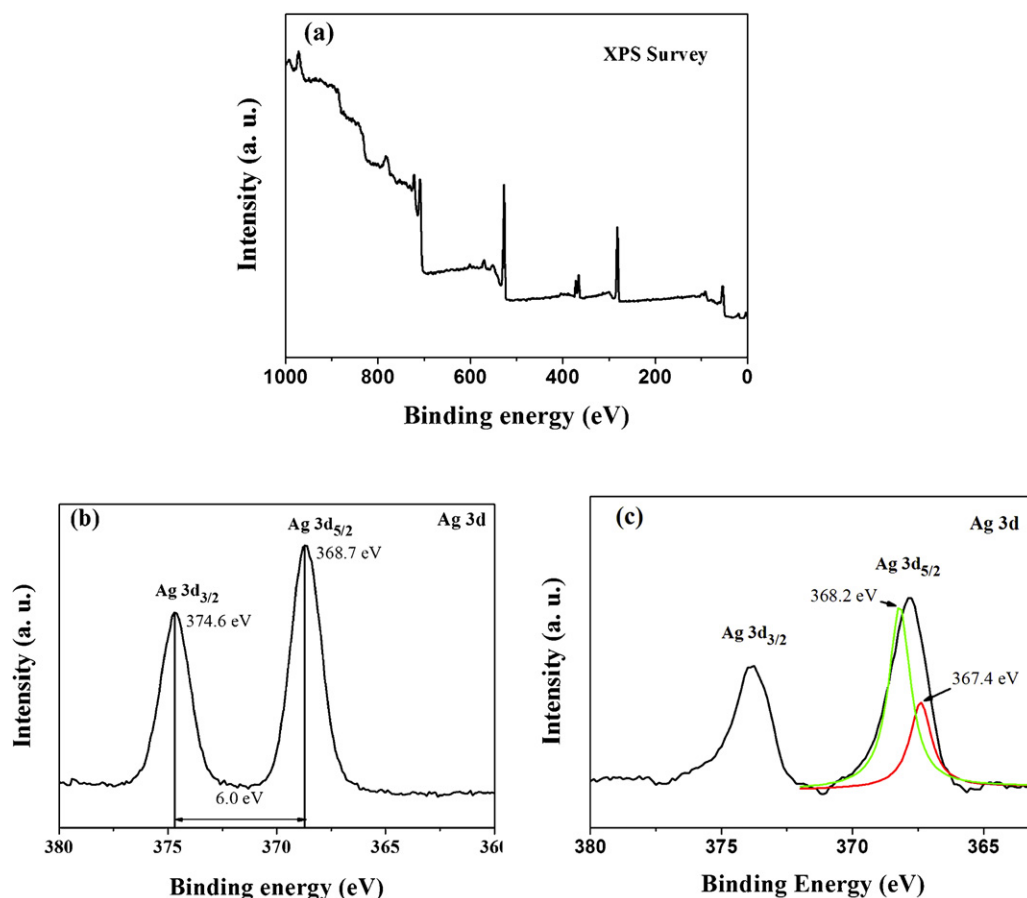


Fig. 8. Cyclic photodegradation of toluene by the Ag/ $\alpha$ -Fe<sub>2</sub>O<sub>3</sub> sample.



**Fig. 9.** XPS spectra of the reused Ag/Fe<sub>2</sub>O<sub>3</sub> (after the fifth operation of photodegradation) and the fresh Ag/Fe<sub>2</sub>O<sub>3</sub> sample. (a) The whole XPS spectrum of the fresh Ag/Fe<sub>2</sub>O<sub>3</sub> sample, (b) the XPS spectrum for the Ag in the fresh Ag/Fe<sub>2</sub>O<sub>3</sub>, and (c) the XPS spectrum for the Ag in the used Ag/Fe<sub>2</sub>O<sub>3</sub>.

The high resolution XPS spectrum of the Ag of the used Ag/Fe<sub>2</sub>O<sub>3</sub> is shown in Fig. 9c, according to which two components of Ag<sub>2</sub>O (367.4 eV) and Ag<sup>0</sup> (368.2 eV) can be found in the used sample [33]. Thus, the Ag particles and Ag<sub>2</sub>O coexist on the surface of the sample after the cyclic photodegradation, the small Ag particles on the Ag/ $\alpha$ -Fe<sub>2</sub>O<sub>3</sub> surface are partially oxidized into Ag<sub>2</sub>O. Moreover, the Ag<sub>2</sub>O prevents further oxidation of the Ag particles on the Ag/ $\alpha$ -Fe<sub>2</sub>O<sub>3</sub> surface. Hence, highly dispersed Ag<sup>0</sup> species would be responsible for the fine stability of the composite Ag/ $\alpha$ -Fe<sub>2</sub>O<sub>3</sub> catalyst. The used catalyst sample of Ag/ $\alpha$ -Fe<sub>2</sub>O<sub>3</sub> still has a certain stability and favorable activity because there still exist Ag<sup>0</sup> species on the surface of  $\alpha$ -Fe<sub>2</sub>O<sub>3</sub> after more reaction cycles.

#### 4. Conclusions

In summary, the prepared hollow and “spindle-like” Ag/ $\alpha$ -Fe<sub>2</sub>O<sub>3</sub> catalyst possesses attractive photovoltage response and remarkable photocatalytic activities in degradation of toluene under xenon lamp irradiation. Due to the well spatial dispersion of Ag species on the “spindle-like”  $\alpha$ -Fe<sub>2</sub>O<sub>3</sub> support, the access of adsorbates toward the Ag sites become more available and thus enhanced catalytic reactivity was achieved.

Furthermore, the complete degradation of toluene occurred without the accumulation of intermediates on the Ag/ $\alpha$ -Fe<sub>2</sub>O<sub>3</sub> surface under the same experimental conditions used as for the individual  $\alpha$ -Fe<sub>2</sub>O<sub>3</sub>, which indicated that the loaded Ag species had a positive effect on the photocatalytic properties. The hollow “spindle-like” Ag/ $\alpha$ -Fe<sub>2</sub>O<sub>3</sub> could be potentially applied in environmental purification utilizing solar energy.

#### Acknowledgments

This work was supported financially by the National Nature Science Foundation of China (NSFC-RGC 21061160495), the National High Technology Research and Development Program of China (863 Program) (No. 2010AA064902), the Major State Basic Research Development Program of China (973 Program) (No. 2011CB936002), the Excellent Talents Program of Liaoning Provincial University (LR2010090) and the Key Laboratory of Industrial Ecology and Environmental Engineering, China Ministry of Education.

#### References

- [1] L.Q. Hao, Z.Y. Wang, F. Li, W.J. Zhang, W. Wang, C.X. Li, L.S. Sheng, *J. Environ. Sci.* 18 (2006) 903–909.
- [2] M.L. Sauer, M.A. Hale, D.F. Ollis, *Photochem. Photobiol. A* 88 (1995) 169–178.
- [3] Y. Luo, D.F. Ollis, *J. Catal.* 163 (1996) 1–11.
- [4] S.A. Larson, J.L. Falconer, *Catal. Lett.* 44 (1997) 57–65.
- [5] T. Ibusuki, K. Takeuchi, *Atmos. Environ.* 20 (1986) 1711–1715.
- [6] T.N. Obee, R.T. Brown, *Environ. Sci. Technol.* 29 (1995) 1223–1231.
- [7] M. Ández-Roma Rafael, C.M. Nelson, *Catal. Today* 40 (1998) 353–365.
- [8] M. Florea, M. Alifanti, V.I. Parvulescu, D. Mihaila-Tarabasau, L. Diamandescu, M. Feder, C. Negriila, L. Frunza, *Catal. Today* 141 (2009) 361–366.
- [9] Z.R. Zhu, X.Y. Li, Q.D. Zhao, H. Li, Y. Shen, G.H. Chen, *Chem. Eng. J.* 165 (2010) 64–70.
- [10] T.N. Obee, *Environ. Sci. Technol.* 30 (1996) 3578–3584.
- [11] J. Zhang, X.H. Liu, X.Z. Guo, S.H. Wu, S.R. Wang, *Chem. Eur. J.* 16 (2010) 8108–8116.
- [12] J. Chen, L.N. Xu, W.Y. Li, X.L. Gou, *Adv. Mater.* 17 (2005) 582–586.
- [13] X.L. Hu, J.C. Yu, J.M. Gong, Q. Li, G.S. Li, *Adv. Mater.* 19 (2007) 2324–2329.
- [14] X.L. Gou, G.X. Wang, X.Y. Kong, D. Wexler, J. Horvat, J. Yang, J. Park, *Chem. Eur. J.* 14 (2008) 5996–6002.
- [15] H.T. Sun, C. Cantalini, M. Faccio, M. Pelino, M. Cantalano, L. Trapfer, *J. Am. Ceram. Soc.* 79 (1996) 927–937.

- [16] T. Hyeon, S. Lee, J. Park, Y. Chung, H.B. Na, *J. Am. Chem. Soc.* 123 (2001) 12798–12801.
- [17] J. Fang, A. Kumbhar, W.L. Zhou, K.L. Stokes, *Mater. Res. Bull.* 38 (2003) 461–467.
- [18] G. Sha, T. Wang, J. Xiao, C. Liang, *Mater. Res. Bull.* 39 (2004) 1917–1921.
- [19] C.L. Zheng, X.Y. Li, Q.D. Zhao, Z.P. Qu, X. Quan, *Sep. Purif. Technol.* 67 (2009) 326–330.
- [20] X.L. Li, W.J. Wei, S.Z. Wang, L. Kuai, B.Y. Geng, *Nanoscale* 3 (2011) 718–724.
- [21] X.S. Li, G.E. Fryxell, C.M. Wang, M.H. Engelhard, *Micropor. Mesopor. Mater.* 111 (2008) 639–642.
- [22] H. Xie, Y.Z. Li, S.F. Jin, J.J. Han, X.J. Zhao, *J. Phys. Chem. C* 114 (2010) 9706–9712.
- [23] L. Kronik, Y. Shapira, *Surf. Sci. Rep.* 37 (1999) 1–206.
- [24] S. Ye, L. Fang, Y. Lu, *Phys. Chem. Chem. Phys.* 11 (2009) 2480–2484.
- [25] Y. Tian, T. Tatsuma, *J. Am. Chem. Soc.* 127 (2005) 7632–7637.
- [26] A.J. Maira, J.M. Coronado, V. Augugliaro, K.L. Yeung, J.C. Conesa, J. Soria, *J. Catal.* 202 (2001) 413–420.
- [27] G. Martra, S. Coluccia, L. Marchese, V. Augugliaro, V. Loddo, L. Palmisano, M. Schiavello, *Catal. Today* 53 (1999) 695–702.
- [28] R. Mendez-Roman, N. Cardona-Martinez, *Catal. Today* 40 (1998) 353–365.
- [29] G. Martra, *Appl. Catal. A: Gen.* 200 (2000) 275–282.
- [30] C. Morterra, *J. Chem. Soc. Faraday Trans.* 184 (1986) 1617–1637.
- [31] G. Marci, M. Addamo, V. Augugliaro, S. Coluccia, E. García-López, V. Loddo, G. Martra, L. Palmisano, M. Schiavello, *J. Photochem. Photobiol. A: Chem.* 160 (2003) 105–114.
- [32] H.J. Zhang, X.Y. Li, G.H. Chen, *J. Mater. Chem.* 19 (2009) 8223–8231.
- [33] G.B. Hoflund, Z.F. Hazos, *Phys. Rev. B* 62 (2002) 11126–11133.